Interpretation of the L X-Ray Emission Spectrum of Zr†

M. O. Krause, F. Wuilleumier,* and C. W. Nestor, Jr.
Oak Ridge National Laboratory, Oak Ridge, Tennessee 37830
(Received 28 April 1972)

The Zr L x-ray emission spectrum, obtained by means of photoelectron spectrometry, is interpreted in terms of the initial distribution of single and multiple vacancies, and radiative, Auger, and Coster–Kronig processes. The model calculation reproduces satisfactorily the salient features, such as relative intensities of satellites and emission branches from L_1, L_2, and L_3 subshells. Subshell-vacancy distribution produced by 9-keV electrons is found to be $L_1:L_2:L_3 \approx 0.9:1:2$. Satellites are categorized according to calculated energy differences between diagram and satellite lines, and one class of satellites is found to coincide with diagram lines. Theoretical total rates of Auger transitions are corroborated by measured linewidths, but rates of Coster–Kronig transitions are too high by a factor of about 2. Finally, x-ray transition rates of the K and L series of Zr are calculated in a central-potential model using relativistic Hartree–Slater wave functions. Values agree excellently with Scofield's values. Theoretical and experimental branching ratios of x rays from L_1, L_2, and L_3 subshells are in satisfactory accord.

I. INTRODUCTION

Detailed analysis and interpretation of the complex L x-ray emission spectrum of Zr were aided by two recent developments: the availability of shakeoff probabilities and transition rates of radiative, Auger, and Coster–Kronig processes, and the application of the technique of photoelectron spectrometry to x-ray analysis. This enabled us to set up a model to calculate the spectrum and to obtain numerical results which can be compared with accurate experimental data. The model we introduce takes into account all physical processes that are known to take place during the initial ionization act and the subsequent decay of the inner-shell vacancies, and stresses the role of the satellite x rays.

Most recently, McGuire[1] analyzed the Ag L spectrum in a similar but less elaborate way. He was, however, at a disadvantage since he had to rely on an old albeit time-honored spectrum.[2]

The Zr L x-ray spectrum, which is well resolved in energy and well characterized in intensity, contains a wealth of information. For this reason, we divide the paper into sections each emphasizing a particular aspect of the analysis.

II. EXPERIMENTAL BACKGROUND

The principle of the new technique of x-ray analysis has been described previously,[3] and the experimental details of this study are given elsewhere.[4] Here we point out the essentials only.

X rays were excited by 9-keV electrons and converted into photoelectrons Ne $1s(\mathrm{Zr}L)$, which in turn were dispersed in an electrostatic electron energy analyzer having a resolution of $\Delta E/E = 0.16\%$ in *electron* energy. We display the resulting photoelectron spectrum in Fig. 1. The spectrum of Fig. 1 can also be regarded as the Zr L x-ray spectrum since the function which transforms the photoelectron spectrum into the x-ray spectrum varies slowly with energy, as shown in Ref. 4. Relative intensities $I'_{h\nu}$ of the spectral lines were given in Table I, last column, of Ref. 4, and are repeated in Table I of this paper. These intensities are corrected for target self-absorption (take-off angle is 23°) and are commonly associated with the relative atomic x-ray emission intensities under the prevailing excitation conditions. That this is not entirely correct will become apparent in Secs. IV–VI.

Natural linewidths of the Zr L x rays were derived[3] from the observed widths using the known instrumental function (Gaussian) and the natural line shape (Lorentzian) and subtracting 0.3 eV for the width of Ne $1s$. Deduced values are summarized in Table I, and assigned errors reflect uncertainties in the measurement and the unfolding procedure.

III. LINEWIDTHS, LEVEL WIDTHS, AND TRANSITION RATES

Before probing the spectrum let us examine the linewidth, a datum that is obtained rather directly from the measurement. Theoretically, the linewidth is the sum of the widths of the levels involved in the transition; and the level width is proportional to the radiative, Auger, and Coster–Kronig transition rates, which we shall denote by R, A, and C, respectively. We get, for example, for the L_3 level width $\Gamma(L_3) = \hbar(R_3 + A_3)$; and for the L_1 level width $\Gamma(L_1) = \hbar(R_1 + A_1 + C_1)$. Also for the $L_1 - M_2$ linewidth, $\Gamma(L_1 - M_2) = \Gamma(L_1) + \Gamma(M_2)$. Since $R \ll A$ and $R \ll C$ for transitions from L and M shells of Zr and neighboring elements, and, in addition, $A_1 \ll C_1$ for L_1 and M_1 shells, the level

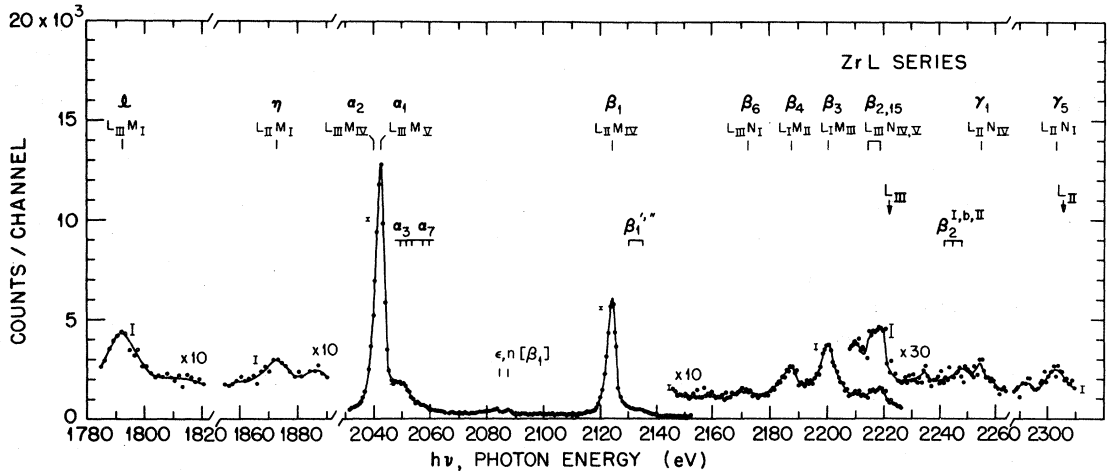

FIG. 1. Zr L x-ray emission spectrum recorded by the technique of photoelectron spectrometry. Spectrum excited by 9-keV electrons and observed at take-off angle of 23°. Notations of lines and satellite structure are conventional. Peaks $\epsilon, \eta[\beta_1]$ are so-called shakeup peaks (Refs. 4 and 19).

widths and, consequently, the linewidths are determined by Coster–Kronig and Auger rates.[5–7] Conversely, measured linewidths allow us to estimate rates of these radiationless transitions from L levels, if $\Gamma(L) \gg \Gamma(M)$, or from M levels, if $\Gamma(M) \gg \Gamma(L)$.

Using the predictions of McGuire[5–7] who made extensive calculations of both L- and M-shell transition rates, we computed the linewidths given in Table I, column 4. Agreement between our experimental and McGuire's theoretical values is good for $L_{2,3} - M_1$ and $L_{2,3} - M_{4,5}$ transitions. This indicates that theoretical total Auger rates of $L_{2,3}$ shells and total Coster–Kronig rates of the M_1 shell are satisfactorily predicted, if we accept what appears to be a reasonable value for $\Gamma(M_{4,5})$; $\Gamma(M_{4,5}) = 0.1$ eV is small compared with $\Gamma(L_2) = 1.8$ eV and $\Gamma(L_3) = 1.5$ eV. In principle, measured linewidths can be expected to be broader than required by the rates of the various decay processes. For example, a diagram line can be subject to broadening by satellite interference, as will be shown in Secs. IV and VI. Findings on Zr are corroborated by the good accord of experimental and theoretical widths of L_2 and L_3 levels of other elements in the medium-Z region, such as Ag,[2] Kr,[8] and Xe.[9] Invoking ω_3 fluorescence yield data,[5] we can then conclude that theory predicts the radiative rate R_3 around $Z = 40$ with about the same accuracy, 20%, as the Auger rate A_3.

The situation is different with transitions to the L_1 level. We measure $\Gamma(L_1 - M_{2,3}) = 5.7(4)$ eV and McGuire calculates 10.7 eV. If we adopt the theoretical $\Gamma(M_{2,3}) = 2.4$ eV, we get $\Gamma(L_1)_{\text{th}} \approx 2.5\ \Gamma(L_1)_{\text{expt}}$. and with $C_1 \gg A_1 \gg R_1$, we get $C_{1,\text{th}} \approx 2.5\, C_{1,\text{expt}}$. If we adopt $\Gamma(M_{2,3}) \lesssim 1$ eV, arguing both $\Gamma(M_{2,3})$ and $\Gamma(L_1)$ are too large for the same reason yet to be explored, we still get $C_{1,\text{th}} \approx 2\, C_{1,\text{expt}}$. Similar gross overestimates of $\Gamma(L_1)$, and therefore C_1, have been noted before for the elements Ag,[2] Kr,[8] and Xe.[9] We suspect the major error to lie with the rates of $L_1 - L_{2,3}M$ (denoted C_{1M}), since they amount to 80–90% of all Coster–Kronig transitions and since they would be the most sensitive to small changes in the energy of the outgoing electron. For Zr, the energy of $L_1 - L_3M_5$ is only about 100 eV and, due to the strong dependence on energy, the rate would change drastically with an uncertainty of some 10 eV in the theoretical energy. However, the energy uncertainty is probably not the only reason for the discrepancy between theory and experiment. Cor-

TABLE I. Experimental and theoretical linewidths (full width at half-maximum) in eV and line intensities, normalized to $I(L\alpha_1) = 100$, of Zr L x rays excited by 9-keV electrons. $I'_{h\nu}$ are apparent intensities of emission lines deduced from the spectrum of Fig. 1 according to Ref. 4; $I_{h\nu}$ are the true intensities corrected for satellite interference.

Line	Energy[a] (eV)	Width, FWHM (eV) Expt	Theory[b]	Relative Intensity $I'_{h\nu}$	$I_{h\nu}$
lL_3-M_1	1792.0	8.6(8)	8.0	4.2(7)	4.2(7)
$\alpha_2 L_3$-M_4	2039.9	...	1.6	11[c]	11[c]
$\alpha_1 L_3$-M_5	2042.4	1.7(3)	1.6	100.0	100.0
$\beta_6 L_3$-N_1	2171.2	6(1)	...	0.9(2)	0.9(2)
$\beta_2 L_3$-N_4	2219.4	[6.5(6)][d]	...	1.6(3)	1.6(3)
ηL_2-M_1	1876.5	8(1)	8.0	2.1(4)	2.3(4)
$\beta_1 L_2$-M_4	2124.4	2.0(3)	1.9	47.5(3.3)	51.6(3.5)
$\gamma_5 L_2$-N_1	2255.1	7(1)	...	0.8(2)	0.9(2)
$\gamma_1 L_2$-N_4	2302.7	...	...	1.8(5)	2.0(5)
$\beta_4 L_1$-M_2	2187.3	5.9(6)	10.7	3.5(5)	4.2(6)
$\beta_3 L_1$-M_3	2201.0	5.5(6)	10.7	5.5(5)	6.5(6)

[a] J. A. Bearden, Ref. 12.
[b] E. J. McGuire, Refs. 5–7.
[c] Inferred.
[d] Width of band.

relation effects are likely to be important. Other calculations[10] using different single-electron wave functions yield Coster–Kronig rates which are not too different from McGuire's. A reexamination of the factors that influence Coster–Kronig rates seems to be indicated.

IV. SATELLITE LINES; ORIGIN AND CLASSIFICATION

A crucial preliminary to the analysis of the spectrum concerns the satellite lines, their origins and their positions relative to the parent lines. Satellites are defined as x rays arising from a one-electron jump in a multihole configuration.

The two sources of satellites are shakeoff and Coster–Kronig processes. Shakeoff occurs during the initial ionization event and creates additional holes predominantly in the outer shells; Coster–Kronig processes transfer initial L_1 vacancies to L_2 and L_3 shells, and L_2 vacancies to L_3 shell, and create an additional hole predominantly in the innermost shell that can take part energetically. We have, in effect, different types of hole states, the LM and the LN states. Let us now see whether the two different hole states lead to two different, distinguishable classes of satellites.

Using relativistic Hartree-Slater wave functions,[11] we calculated the energies of diagram and satellite x rays from the differences of the total energies of initial and final states and then formed the energy differences between satellites and parent diagram lines. For example, we obtain an energy difference of 7.5 eV for $\Delta E = (L_3M_5 - M_5M_5) - (L_3 - M_5)$. A set of typical values is tabulated in Table II. It can be seen at once that we have one class of satellites from LM states which lie above their parent lines by at least 7 eV, and a second class from LN states which are very close, often within 0.4 eV, to their parent lines. The first class is separated from the diagram lines, while the second class, even with negligible instrumental line broadening, is too close to the diagram lines to be distinguishable. There is a borderline case, $[L_3N - NN] - [L_3 - N]$, with shifts between 1 to 5 eV, but if we consult Table I for the linewidths we see that these satellites are hidden, too. It follows then, that most shakeoff events lead to satellites indistinguishable from the diagram lines, and most Coster–Kronig events lead to observable satellites. The latter class was documented a long time ago, and was, in fact, associated with the radiationless transitions that Coster and Kronig postulated.

We estimate the accuracy of the calculated energy shifts to be better than 1 eV judging from the self-consistency criteria we impose ($\approx 10^{-5}$), from comparison of theoretical x-ray energies with those quoted by Bearden,[12] and especially from the comparison of calculated and experimental shifts of the satellites accompanying $L\alpha_{1,2}$ and $L\beta_1$. We calculate a shift of about 7.5 eV and observe a mean displacement of about 8 eV for the satellite structure. Earlier measurements yielded[13] 6.5 eV to 10.6 eV for α_3 to α_5 respectively, 5.8 eV for β_1' and 11.0 eV for β_1''. The $\alpha_{6,7}$ satellites near $\Delta E = 15$ eV are probably due to transitions in triple-hole (LMM) states. The spread of the satellites over several eV is ascribed to multiplet splitting[14] which our calculation ignores. Presumably, the calculation gives the weighted mean energy of the components.

TABLE II. Energy shift (in eV) of radiative transitions to the L shell in the presence of an additional hole in M and N shells. For example: $\Delta E = 7.8$ eV for $(L_3M_4\text{-}M_5M_4)\text{-}(L_3\text{-}M_5)$. Values calculated in relativistic Hartree–Slater potential model.

Diagram or parent line	Shell with one additional hole					
	M_3	M_4	M_5	N_1	N_3	N_4
$L_1\text{-}M_2$	6.5	...		...	0.3	...
$L_1\text{-}M_3$	7.1	...	8.4	...	0.3	0.2
$L_1\text{-}N_3$	23.0	...	24.6	...	2.7	1.2
$L_3\text{-}M_1$	7.7	...	8.2	...	0.4	0.2
$L_3\text{-}M_4$	...	7.6	7.3	0.4	0.4	...
$L_3\text{-}M_5$[a]	7.5	7.8	7.5	0.4	0.4	0.2
$L_3\text{-}N_1$	...	23.8	23.4	2.8	2.2	0.9
$L_3\text{-}N_4$	26.8	...	27.7	5.4	4.5	2.4

[a] With another hole in M_1 shell $\Delta E = 6.8$ eV.

Results presented in Table II bear out findings on "chemical-shift" effects on x rays: If an electron is removed from the valence shell or any other shell that lies above the shells involved in the radiative transition, the line shift is minimal. We calculate a shift of 0.2–0.4 eV for $\Delta E = (LN - MN) - (L - M)$, while chemical shifts of x rays are a few tenths of an eV at most.[15] The basic reason for the small shifts between these x rays is the fact that inner levels are displaced by almost the same amount.[16]

Perhaps the most significant result of this analysis of x-ray satellites is the conclusion that a large class of satellites merges into the diagram lines. Some of the consequences will be discussed in Secs. V and VI.

V. SYNTHESIS OF THE X-RAY SPECTRUM: MODEL CALCULATION

We introduce a model which should allow us to reproduce the salient features of the emission spectrum. The model takes into account: (a) the initial vacancy production L_1, L_2, and L_3, and the concomitant shakeoff process with probabilities P_1, P_2, and P_3; (b) intra-L-shell hole transfer by Coster–Kronig transitions with the yields $f_{1,2}, f_{1,3}$, and $f_{2,3}$; (c) distinction between satellite lines arising from LM and LN hole states; (d) hole decay by radiation with total rates R_1, R_2, and R_3 or by

Auger processes with total rates A_1, A_2, and A_3; and (e) alternate decay channels of double-hole states according to the pertinent transition probabilities.

Then the number of diagram x rays originating from single-hole states in the L subshells is given by

$$n_1(L_1) = \frac{R_1}{A_1+R_1}(1-P_1)(1-f_{1,2}-f_{1,3})L_1 , \quad (1a)$$

$$n_2(L_2) = \frac{R_2}{A_2+R_2}(1-P_2)(1-f_{2,3})L_2 , \quad (1b)$$

$$n_3(L_3) = \frac{R_3}{A_3+R_3}(1-P_3)L_3 . \quad (1c)$$

The number of satellite x rays originating from double hole states in LX shells ($X=M$ and N) is given by

$$n_1'(L_1X) = \frac{R_1'}{A_1+R_1'}P_1(1-f_{1,2}-f_{1,3})L_1 , \quad (2a)$$

$$n_2'(L_2X) = \frac{R_2'}{A_2+R_2'}[P_2(1-f_{2,3})L_2 + f_{1,2}(1-P_1)(1-f_{2,3})L_1] , \quad (2b)$$

$$n_3'(L_3X) = \frac{R_3'}{A_3+R_3'}[P_3L_3+f_{2,3}(1-P_2)L_2 + f_{1,3}(1-P_1)L_1] . \quad (2c)$$

Finally, the small but not negligible number of satellites originating from triple-hole states of the type LXX ($X=M$ and N) is given by

$$n_1''(L_1XX) = 0 , \quad (3a)$$

$$n_2''(L_2XX) = \frac{R_2''}{A_2+R_2''}f_{1,2}P_1L_1 , \quad (3b)$$

$$n_3''(L_3XX) = \frac{R_3''}{A_3+R_3''}[f_{1,3}P_1L_1 + f_{1,2}f_{2,3}(1-P_1)L_1+P_2f_{2,3}L_2] . \quad (3c)$$

In Eqs. (1)–(3), we have foregone the use of the fluorescence yield, and disregarded multiple shakeoff and changes of rates with the number of holes, except for the radiative rates, where we used $R' = 1.1R$ and $R'' = 1.2R$ (cf., Sec. VII). We also have ignored, for the moment at least, redistribution of double holes before emission of x rays from the L shell.

Recalling the conclusions of Sec. IV on satellites, the number of "true" diagram and satellite x rays given by the relations (1)–(3) cannot be counted separately. Part of the satellites, Eqs. (2) and (3), coincide with the diagram lines and part do not. We can observe those satellites only that arise from LM states, and so-called diagram lines that are contaminated by satellites which arise from LN states.

To arrive at quantities that can be compared with experiment, we need to divide the satellites into components, that is, we divide the radiative holes $n'(LX)$ into $n'(LM)$ and $n'(LN)$ holes by splitting the total shakeoff probability P into partial probabilities P_M and P_N, with $P=P_M+P_N$, and total Coster–Kronig yields f into partial yields f_M and f_N, with $f=f_M+f_N$. Similarly, we partition $n''(LXX)$ into $n''(LMM+LMN)$ and $n''(LNN)$. As an example of the procedure we subdivide $n_3'(L_3X)$ of Eq. (2c). The number of satellites from double hole states that are separated from the parent lines is then given by

$$n_3'(L_3M) = \frac{R_3'}{A_3+R_3'}[P_{3M}L_3+f_{1,3M}(1-P_1)L_1] \quad (4a)$$

since $f_{2,3M}=0$, and the corresponding number of satellites that coincide with the parent lines is given by

$$n_3'(L_3N) = \frac{R_3'}{A_3+R_3'}[P_{3N}L_3+f_{2,3}(1-P_2)L_2 + f_{1,3N}(1-P_1)L_1] , \quad (4b)$$

with $f_{2,3}=f_{2,3N}$.

Following this satellite decomposition we can formulate equations for several *observable* quantities: (i) Intensity ratio of satellite structure, designated β_1''', to $L\beta_1$ line

$$\frac{I'(\text{sat})}{I'(\beta_1 \text{ line})} = \frac{n_2'(L_2M)+n_2''(L_2MM+L_2MN)}{n_2(L_2)+n_2'(L_2N)+n_2''(L_2NN)} . \quad (5a)$$

If all satellites were separable from the parent line, the ratio would be

$$\frac{I(\text{sat})}{I(L_2-M_4)} = \frac{n_2'(L_2X)+n_2''(L_2XX)}{n_2(L_2)} . \quad (5b)$$

This is the "true" ratio. (ii) Intensity ratio of satellite structure, designated α_3 to α_7, to $L\alpha_{1,2}$ line

$$\frac{I'(\text{sat})}{I'(\alpha_{1,2}\text{ line})} = \frac{n_3'(L_3M)+n_3''(L_3MM+L_3MN)}{n_3(L_3)+n_3'(L_3N)+n_3''(L_3NN)} . \quad (6a)$$

The corresponding "true" ratio would be

$$I(\text{sat})/I(L_3-M_{4,5}) = [n_3'(L_3X)+n_3''(L_3XX)]/n_3(L_3) . \quad (6b)$$

(iii) Intensity ratio of emission branches

$$\sum_{L_1} I_{h\nu}' : \sum_{L_2} I_{h\nu}' : \sum_{L_3} I_{h\nu}' = [n_1(L_1)+n_1'(L_1N)] : [n_2(L_2)+n_2'(L_2N)+n_2''(L_2NN)] : [n_3(L_3)+n_3'(L_3N)+n_3''(L_3NN)] . \quad (7a)$$

If we had pure diagram lines only, the right-hand

TABLE III. Variation of several observable features of Zr L spectrum with changes of initial hole distribution, total and partial rates of Coster–Kronig transitions and alternate decay routes for LM hole states. Experimental values in bottom row. Intensity ratios are given in percent.

Case No.	Vacancy distribution $L_1:L_2:L_3$	Coster–Kronig rates[a]	Sat/$L\beta_1$ Eq. (5b) True	Sat/$L\beta_1$ Eq. (5a) Obs.	Sat/$L\alpha_{1,2}$ Eq. (6b) True	Sat/$L\alpha_{1,2}$ Eq. (6a) Obs.	Branches of $L_1:L_2:L_3$ shells Eq. (7a)
1	1:1:2	$1C_{th}$	47.6	18.2	81.7	38.2	6.6:47.3:100
2	1:1:2	$0.5C_{th}$	45.0	16.4	71.8	35.1	12.1:51.8:100
3	0.5:1:2	$1C_{th}$	35.6	10.9	57.0	21.5	3.3:47.0:100
4	0.5:1:2	$0.5C_{th}$	34.5	10.0	50.2	19.5	6.1:51.4:100
5	0.5:1:2	$0.5C_{1,th}$	34.9	11.4	54.1	19.1	5.8:47.1:100
6	1:1:2	$0.5C_{1M,th}$	48.0	15.4	75.9	31.8	10.8:47.8:100
7	0.6:1:2	$0.33C_{1M,th}$	38.3	9.5	56.2	18.1	8.4:47.6:100
8	0.5:1:2	$0.5C_{1M,th}$	35.8	9.6	54.1	17.9	5.5:47.2:100
9	0.5:1:2	$0.33C_{1M,th}$	35.8	8.5	52.0	15.6	7.0:47.4:100
10	1:1:2	0.5;0.3	48.0	10.3	75.9	20.2	9.8:45.4:100
11	1:1:2	0.5;0.5	48.0	7.2	75.9	13.7	9.4:44.4:100
12	0.9:1:2	0.5;0.3	45.3	9.5	71.1	18.8	9.0:45.9:100
13	0.8:1:2	0.5;0.3	43.3	8.9	67.2	17.0	8.1:45.8:100
14	0.8:1:2	0.5;0.5	43.3	6.2	67.2	11.6	7.8:44.8:100
15	0.6:1:2	0.5;0.3	38.3	7.3	58.5	13.7	6.3:46.0:100
Experiment[b]				8.7		18	8.8:44.4:100
$\pm\sigma$				1.2		2	0.6 3.3

[a] C_{th} = all Coster–Kronig rates; $C_{1,th}$ = only $L_1L_{2,3}$ X rates; $C_{1M,th}$ = only $L_1L_{2,3}$ M rates; cases Nos. 10–15 use 0.5 $C_{1M,th}$ and $A_{M\text{-}NN}/R_{2,3}$ = 0.3 or 0.5. $A_{M\text{-}NN}$ = Auger rate for $M_{4,5}$ shell and $R_{2,3}$ = radiative rate for $L_{2,3}$ shell.

[b] Branch intensities from Table I; $I'(L_1N_{2,3}) = 1.3$ added.

side of Eq. (7a) would read

$$n_1(L_1):n_2(L_2):n_3(L_3)\ . \tag{7b}$$

In Eq. (7a), we neglected a few cases (i.e., $L_{2,3}-M_1$) for which the shift $\Delta E = E(\text{sat}) - E(\text{line})$ is slightly less than the natural linewidth, while otherwise we placed the dividing line at $\Delta E = \Gamma(\text{line})$, full width at half-maximum. This choice of the dividing line is reasonable, since instrumental line broadening is small.

It should be noted that the ratios given by Eqs. (5) and (6) are influenced by the rates R and A only through the Coster–Kronig yields, while the ratios given by Eq. (7) are weighted by $R/(A+R)$.

Numerical results were obtained relying on McGuire's theoretical total rates[5] R_i and A_1, $i = 1, 2$, and 3, and our estimate[17] of the shakeoff probabilities $P_1 = P_2 = P_3 = 0.18$, with $P_M = 0.03$ and $P_N = 0.15$. We used also McGuire's theoretical Coster–Kronig rates,[6] both total and partial, as a starting point to derive $f_{1,2}, f_{1,2M}, f_{1,2N}, f_{1,3}$, etc., and then changed these rates (and f values) in such a manner to be compatible with the observed linewidths, see Sec. III. In the absence of theoretical predictions[18] for the initial vacancy distribution created by 9-keV electrons, we considered $L_1:L_2:L_3$ variable, maintaining however $L_2:L_3 = 1:2$.

In Table III, we compare the numerical results of the various relations given by Eqs. (5)–(7) with the experimental data, and at the same time show to which extent changes in the different parameters influence the spectral features. We first display the results obtained with the theoretical Coster–Kronig rates, and two different populations of $L_1:L_2:L_3$. Agreement with experiment is poor, cases 1 and 3. Reduction of all Coster–Kronig rates to $0.5\,C_{th}$ leads to improvement, case 4. Reduction of C_1 only, which is required by $\Gamma(L_1)$, changes the results slightly, case 5. Reduction of C_{1M} only, which follows from arguments presented in Sec. III, leads to the ratios of cases 6–9. A very good over-all result is achieved with $L_1:L_2:L_3 = 0.6:1:2$ and $0.33\,C_{1M,th}$ case 7. However, $0.33\,C_{1M,th}$ appears to be too drastic a reduction in view of the findings in Sec. III and, more important yet, case 7 makes no allowance for the possibility of alternate decay routes of LM double holes. If the M hole were to decay prior to the *radiative* decay of the L hole, a redistribution of the satellites would be the consequence. According to Refs. 5–7, the decay probability of an $M_{4,5}$ hole, predominantly by an $M_{4,5}-NN$ Auger process, is about the same as the probability of an $L_{2,3}$ hole to decay by a radiative transition, the type of transition we are measuring. Therefore, intensity is taken away from $LM_{4,5}$-$XM_{4,5}$ lines and transferred to $LNN-XNN$ lines, $X = M$ or N, leading to an increase in the intensity of invisible

satellites at the expense of intensity of observable satellites. In cases 10–15, this refinement of the model is taken into account using $0.5\,C_{1M,\mathrm{th}}$, and using values of 0.3 and 0.5 for the probability $P_{M\text{-}NN} = A_{M\text{-}NN}/R_{2,3}$ ($A_{M\text{-}NN}$ is the Auger rate for $M_{4,5}$–NN, and $R_{2,3}$ is the total radiative rates for $L_{2,3}$ shells). Case 12 yields the best over-all agreement with experiment. At this stage, one can only speculate as to why $P_{M\text{-}NN} = 0.3$ gives a better result than the theoretical prediction of about 0.5.

While the synthesis of the spectrum is perhaps not as perfect as one might wish, it is gratifying to see that no serious discrepancy occurs anywhere. Especially noteworthy is the fact that major steps taken in the model calculation, such as reduction of Coster–Kronig rates, division of satellites into two classes and inclusion of shakeoff, are backed by independent data. Were we not to partition the satellites, we would get satellite intensities of 70 and 45% of the $L\alpha_{1,2}$ and $L\beta_1$ line intensities respectively, in clear contradiction to the experimental observation. The initial vacancy distribution suggested by this calculation should be confirmed by further experimentation and accurate calculations of subshell ionization cross sections under electron impact. This analysis suggests $L_1 : L_2 : L_3 = (0.8 \text{ to } 1.0) : 1 : 2$ for Zr and 9-keV electrons.

VI. DIAGRAM LINES

What is commonly regarded as a diagram line is in fact a composite line, consisting of the "pure" diagram line, arising from a single-electron jump in a single-hole state according to definition, and a certain class of satellites which might appropriately be called parasites. This follows from the results of Secs. IV and V. As an example, line $L\beta_1$ is composed of the pure line $L_2 - M_4$ and the satellites $L_2N - M_4N$ and $L_2NN - M_4NN$. The relative contributions of the components are derived from Eqs. (1)–(4) as follows:

$$I(\beta_1 \text{ line}) \propto n_2(L_2) + n_2'(L_2N) + n_2''(L_2NN)\,, \tag{8}$$

if the L_2 hole of the $L_2M_{4,5}$ state always decays before the $M_{4,5}$ hole. Otherwise, the term

$$P_{M\text{-}NN}[n_2'(L_2M) + n_2''(L_2MM + L_2MN)] \tag{9}$$

must be added with $P_{M\text{-}NN} \approx 0.3$ according to Table III. To give an idea of the magnitude of the various contributions, we list in Table IV the compositions of $L\alpha_{1,2}$, $L\beta_1$, and $L\beta_3$ lines for case No. 12 of Table III, which gave best agreement with experiment. Between 17 and 30% of the line intensities are due to satellites, with shakeoff contributing the greater part. Other lines originating in the L_3, L_2, and L_1 levels are partitioned in the same way as the $L\alpha_{1,2}$, $L\beta_1$, and $L\beta_3$ lines, respectively, for, considering linewidths and satellite shifts, lines from the same subshells are affected similarly. For the sake of completeness, the composition of *observable* satellites is also displayed in Table IV; in this instance, Coster–Kronig processes contribute the greater part of the intensity. Also given in Table IV is the composition of all (true) satellites. Shakeoff and Coster–Kronig processes contribute about equally for the spectrum reported. Generally, satellite contributions vary with the initial vacancy distribution, which depends on the excitation mode, with shakeoff probabilities and with total and partial Coster–Kronig rates. Even in the absence of Coster–Kronig events, systematics of shakeoff[19] suggest the presence of substantial satellite interference for x-ray lines of any series, except for K-series lines of the first row elements, where satellites have been studied the most thoroughly, and for lines originating in the penultimate principal shell. In such cases all satellites are isolated.

Consequences of this result are manifold. We mention the possibility of intensity reduction of observable satellites, errors in the measurement of absolute and relative intensities and distortion of line shapes,[20] which includes asymmetry, non-Lorentzian contour and broadening. In unfavorable cases, branching ratios can also be altered. Returning to the Zr L spectrum, relative intensities $I'_{h\nu}$ of Table I have to be corrected, according to Table IV, by factors of 0.694 for L_3 lines, 0.754 for L_2 lines, and 0.825 for L_1 lines, to remove satellite interference. Following this correction, intensities $I_{h\nu}$, tabulated in the last column of Table I, represent the relative intensities of the

TABLE IV. Composition of so-called diagram lines and satellite lines for the "best" case No. 12 of Table III. Percentages are given of pure diagram lines, and of satellite lines from shakeoff (SO) and Coster-Kronig (CK) processes.

Category	Number of holes[a]	$L\alpha_1$ (L_3 shell)	$L\beta_1$ (L_2 shell)	$L\beta_3$ (L_1 shell)
		"Diagram" lines		
pure	1	69.4	75.4	82.5
SO	2 (3)	14.8	15.7	17.5
CK	2 (3)	12.5	7.2	0
SO+CK	3 (4)	3.3	1.7	0
		Observable satellite lines		
CK	2	69.9	60.7	0
SO	2	10.5	21.0	100
SO+CK	3	19.6	18.3	0
		True (all) satellite lines		
CK	2 (3)	51.8	38.0	0
SO	2 (3)	34.0	51.8	100
SO+CK	3 (4)	14.2	10.2	0

[a]Numbers in parentheses give the number of holes that are present when the $M_{4,5}$ hole decays prior to the radiative decay of the L hole in the $LM_{4,5}$ double-hole state.

TABLE V. Calculated x-ray transition rates in Zr (in units of eV/$\hbar$) using neutral atom wave functions; $2.45(-4) = 2.45\times10^{-4}$.

Final hole	Initial hole K	L_1	L_2	L_3
L_2	0.7862	...	...	...
L_3	1.504	2.45(−4)	...	...
M_1	...	...	1.48(−3)	1.68(−3)
M_2	0.1186	9.84(−3)	...	...
M_3	0.2310	1.71(−2)	...	...
M_4	4.948(−4)	...	4.50(−2)	4.38(−3)
M_5	7.037(−4)	...	...	3.89(−2)
N_1	...	...	2.40(−4)	2.71(−4)
N_2	1.599(−2)[a]	1.42(−3)	...	...
N_3	3.109(−2)	2.50(−3)	...	...
N_4	...	...	2.75(−3)	2.65(−4)

[a]Scofield's value (Ref. 22) presumably is 0.0160 rather than 0.106 due to the possibility of a misprint.

pure diagram lines of the Zr L emission spectrum.

VII. THEORETICAL EMISSION RATES AND L BRANCHING RATIOS

A stringent test of a theoretical model can be made by comparing the *partial* radiative rates with experimental data, even though the data may only be relative. In this section, we present calculated Zr x-ray emission rates and compare theoretical and experimental L branching ratios.

We used the method of Lu *et al.*[21] which treats the electrons as moving in a central potential given by the relativistic Hartree–Slater theory[11] and which includes higher multipoles and retardation. Transition rates were calculated for both the K and the L series and are listed in Table V. This calculation agrees excellently with Scofield's,[22] which is based on the same model.[23] The only difference occurs in transitions to the N_4 level which may be due to Scofield's placing of one electron into the N_5 subshell. Variation of the Slater parameter ϕ between 1.0 and 1.5 would produce a rate change of not more than 50%, as a test calculation showed. We also computed the rate for the satellite transition L_3M_4–M_4M_4 and obtained 5.00×10^{-3} eV/$\hbar$, which is 11% greater than the rate for $L_3 - M_4$. This is a somewhat greater enhancement than given by the (approximate) Z^4_{eff} dependence of radiative rates.

Finally, in Table VI, we compare theoretical branching ratios with experimental ratios taken from the last column of Table I. We note satisfactory agreement, except for the weak transition $L_2 - N_1$. Agreement for $L_{2,3} - N_4$ transitions is surprisingly good if we consider that theory deals with the free atom and experiment with the solid where N_4 electrons are part of the band structure. The radiative decay scheme of Zr L is displayed in Fig. 2 for ready visualization.

The theory used by Scofield and by us was shown earlier to yield generally satisfactory results when checked against measured intensity ratios of selected lines of the L series[24] of elements with $Z > 57$, and of the K series[25] of elements with $Z \geq 18$. We consider the agreement satisfactory for lines originating in the same subshell if intensity ratios are predicted within ±20% for lines having the final hole in the same shell, and within ±50% for lines having the final hole in different principal shells. On the surface the accord between theory and experiment seems surprising, since no corrections for satellite interference were applied to the data of Refs. 24 and 25, some of which were obtained with poor instrumental resolution. However, as

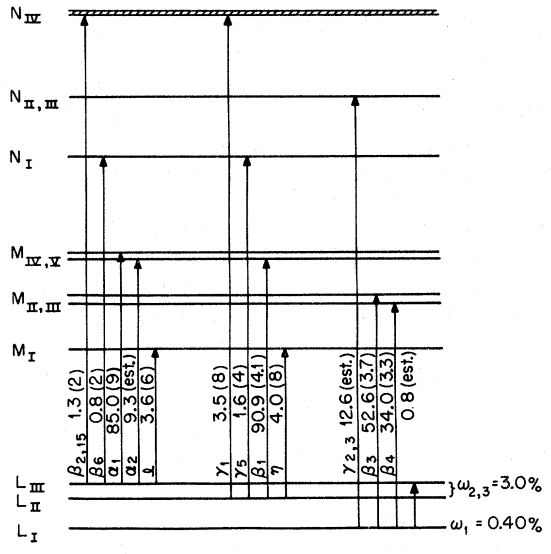

FIG. 2. Experimental branching ratios of x rays originating, respectively, in the L_1, L_2, and L_3 shells of zirconium. Estimated values are taken from theory.

TABLE VI. Comparison of experimental and theoretical branching ratios of x rays from L_1, L_2, and L_3 subshells. Each branch is normalized to 100.0.

Transition	Theory	Experiment
L_3-M_1	3.7	3.6(6)
L_3-M_4	9.6	9.3[a]
L_3-M_5	85.5	85.0(9)
L_3-N_1	0.6	0.8(2)
L_3-N_4	0.6	1.3(2)
L_2-M_1	3.0	4.0(8)
L_2-M_4	90.9	90.9(4.1)
L_2-N_1	0.5	1.6(4)
L_2-N_4	5.6	3.5(8)
L_1-L_3	0.8	0.8[a]
L_1-M_2	31.6	34.0(3.3)
L_1-M_3	55.0	52.6(3.7)
L_1-$N_{2,3}$	12.6	12.6[a]

[a]Inferred from theory.

pointed out in Secs. IV–VI, relative satellite intensities are about the same if the x rays originate in the *same* subshell, so that a bias of more than 10% should seldom be introduced. But when accuracy is required to be sure that no serious bias exists, it is imperative to evaluate the satellite contributions.

VIII. CONCLUDING REMARKS

While we demonstrated in the companion paper, Ref. 4, that an x-ray spectrum can be measured with accuracy by photoelectron spectrometry, we have shown in this analysis of the Zr L emission spectrum that the spectrum can be satisfactorily interpreted in terms of all physical processes that take place during initial creation and subsequent decay of inner shell vacancies. Out of a number of conclusions that emerged in the course of the analysis we should like to emphasize the most significant ones in this final section.

Multiple-hole configurations lead to x-ray satellites which may or may not be distinguishable from the parent diagram lines. In general, Coster-Kronig satellites appear on the high-energy side of the parent lines and shakeoff satellites coincide with the parent lines. However, due to the competitive decay of individual holes in multiple-hole configurations, a fraction of the high-energy satellites can be transferred to the region beneath the parent lines. These consequences of multihole states are not restricted to the case of the Zr L spectrum, where under 9-keV electron excitation satellites account for about 40% of the spectral intensity, and need be considered whenever x-ray line shapes and linewidths are investigated and whenever intensities and energies of so-called diagram lines are measured.

A reexamination of the theory of Coster–Kronig transitions is indicated. In the region around $Z=40$, rates of transitions to the L_1 shell are overestimated by a factor of about 2.

In contrast to the difficult calculations of Coster–Kronig rates, calculations of partial radiative transition rates appear to be quite satisfactory. Using a relativistic version of the Herman–Skillman method, theory yields values generally in good agreement with experiment.

Finally, having understood a spectrum as complex as the Zr L spectrum, we can then utilize this and other x-ray emission spectra to study, for example, details of the ionization process as a function of energy and excitation mode. There is a paucity of data and a need for better understanding of differential inner-shell ionization phenomena by electrons and particles.

ACKNOWLEDGMENT

We are indebted to Dr. E. J. McGuire for sending us preprints and reports prior to publication.

†Research sponsored by the U. S. Atomic Energy Commission under contract with Union Carbide Corporation.

*On leave from Laboratoire de Chimie Physique de l'Université Paris VI, France.

[1]E. J. McGuire, Phys. Rev. A 5, 1043 (1972); 5, 1052 (1972).

[2]L. G. Parratt, Phys. Rev. 54, 99 (1938). This excellent measurement remained unsurpassed for several decades.

[3]M. O. Krause, Chem. Phys. Letters 10, 65 (1971). For Ne 1s, $\Gamma=0.3$ eV.

[4]M. O. Krause and F. Wuilleumier, Proceedings of International Conference on Inner Shell Ionization Phenomena, Atlanta, Ga. (unpublished).

[5]L shell: E. J. McGuire, Phys. Rev. A 3, 587 (1971). An exhaustive bibliography of existing calculations is given by P. V. Rao, M. H. Chen, and B. Crasemann, *ibid.* 5, 997 (1972).

[6]L shell: E. J. McGuire, Phys. Rev. A 3, 1801 (1971).

[7]M shell: E. J. McGuire, Phys. Rev. A 5, 1043 (1972).

[8]F. Wuilleumier, J. Phys. (Paris) 32, C4-88 (1971).

[9]F. Wuilleumier, thesis (University of Paris, 1969) (unpublished).

[10]B. Crasemann, M. H. Chen, and V. O. Kostroun, Phys. Rev. A 4, 2161 (1971); compare B. Talukdar and D. Chattarji, *ibid.* 1, 33 (1970).

[11]C. C. Lu, T. A. Carlson, F. B. Malik, T. C. Tucker, and C. W. Nestor, Jr., Atomic Data 3, 1 (1971).

[12]J. A. Bearden, Rev. Mod. Phys. 39, 78 (1967).

[13]Y. Cauchois and H. Hulubei, *Table des longueurs d'onde des émissions X et discontinuités absorption* (Hermann et Cie, Paris, 1947).

[14]L. Pincherle [Phys. Rev. 61, 225 (1942)] gives an early detailed account. He also touches upon several subjects treated in the present paper.

[15]*Röntgenspektren and Chemische Bindung*, edited by A. Meisel (VEB Reprocolor, Leipzig, 1966), p. 212; A. Faessler and M. Goehring, Naturwiss. 39, 169 (1952); Y. Cauchois, *Les spectres de rayons X et la structure électronique de la matière* (Gauthier Villars, Paris, 1948).

[16]This calculation; see also T. A. Carlson, in *Electron Spectroscopy*, edited by D. A. Shirley (North-Holland, Amsterdam, 1972), p. 74.

[17]We changed shakeoff probabilities of Kr [M. O. Krause and T. A. Carlson, Phys. Rev. 158, 18 (1967)] for L photoionization according to the systematics given by T. A. Carlson, C. W. Nestor, Jr., T. C. Tucker, and F. B. Malik [*ibid.* 169, 27 (1969)].

[18]Using the universal cross-section curve, calculated for Be to Ne, one would obtain for Zr $L_1:L_2:L_3 \approx 3.6:46:100$ [E. J. McGuire (private communication); and J. Phys. (Paris) 32, C4-37 (1971)]; transferring directly photoionization cross sections one would get $L_1:L_2:L_3=140:50:100$ [E. J. McGuire, Sandia Laboratories Report No. SC-RR-70-721 (1970) (unpublished)].

[19]M. O. Krause, J. Phys. (Paris) 32, C4-67 (1971).

[20]Other sources of line-shape distortion are discussed by J. Finster, G. Leonhardt, and A. Meisel, J. Phys. (Paris) 32, C4-218 (1971); J. W. Cooper and R. E. LaVilla, Phys. Rev. Letters 25, 1745 (1970).

[21]C. C. Lu, F. B. Malik, and T. A. Carlson, Nucl. Phys. A175, 289 (1971).

[22]J. H. Scofield, Phys. Rev. 179, 9 (1969).

[23]This holds when neutral atom wave functions are used. Using wave functions of actual initial and final states instead, rates which are about 5% higher are obtained.

[24]S. I. Salem, R. T. Tsutsui, and B. A. Rabbani, Phys. Rev. A 4, 1728 (1971); J. H. McCrary, L.V. Singman, L. H. Ziegler, L. D. Looney, C. M. Edmonds, and C. E. Harris, *ibid.* 5, 1587 (1972).

[25]P. F. Dittner and C. E. Bemis, Phys. Rev. A 5, 481 (1972); J. H. McCrary, L. V. Singman, L. H. Ziegler, L. D. Looney, C. M. Edmonds, and C. E. Harris, *ibid.* 4, 1745 (1971); V. W. Slivinsky and P. J. Ebert, *ibid.* 5, 1581 (1972).

PHYSICAL REVIEW A VOLUME 6, NUMBER 3 SEPTEMBER 1972

Optimized Pseudostates, Intermediate-Energy Scattering, and Collective Modes in Atoms*

M. H. Mittleman
Physics Department, City College of the City University of New York, New York, New York 10031
(Received 11 April 1972)

In many of the usual methods of calculating scattering amplitudes, a basis set is chosen in which to expand the wave function, and then the coefficients are optimized. We ask here, how does one, in addition, optimize the basis set. A natural outgrowth of the formalism is the concept of an "average inelastic channel" which could, under certain circumstances, be interpreted as a collective mode of excitation of the target.

I. INTRODUCTION

A common technique used to calculate scattering amplitudes of particles off targets with internal degrees of freedom is to choose a finite basis set in which to expand the total wave function and then to optimize the choice via some variational principle. If target eigenstates are chosen as a basis and the coefficients (which are functions of the projectile coordinates) are optimized by the Kohn principle, the result is the usual close coupling equations.[1] Other methods are obtained by a different choice of basis set.[2] These are usually called pseudostate expansions.

More general techniques are obtained by optimizing the choice of basis itself. For example, a parameter can be inserted in the target basis and be allowed to depend upon the projectile position.[3] The parameter can then be determined variationally. More general approaches can be obtained by allowing for more freedom in the basis function.[4]

In this paper we turn our attention to the more general problem of the optimization of an expansion basis. That is, rather than prechoosing the expansion basis, we ask for the best choice of an expansion basis within the restrictions laid down below. The general problem is treated within the context of electron-atom scattering at intermediate energies for physical reasons outlined at the beginning of the next section. The equations which are derived are a nonlinear set, and it is clear that this is a general feature of the technique. The derivation is given in Sec. II without any recognition of the complications introduced by an attempt to conserve total angular momentum. These serve only to becloud the essential points and will be given along with detailed calculations subsequently.

The mathematical considerations outlined above lead to the concept of an "average inelastic channel" (AIC). This has already been shown to be a useful concept in describing elastic scattering.[5,6] We derive an equation defining the AIC and, in the last section, discuss its approximate solutions. The possibility that it represents a collective mode of excitation of the target is discussed, and some crude estimates of the energy and width of the state are made.

II. INTERMEDIATE ENERGY ELECTRON-ATOM SCATTERING

At intermediate energies (where neither high nor low-energy expansion techniques are expected to work), it seems unlikely that scattering will be easily describable by a systematic expansion technique. That is, the problem of preselecting an expansion basis such that the inclusion of only a few of them will give an adequate description of this scattering does not seem to be solvable now. An alternate approach is the optical potential method.[7] If one keeps only up to second-order